Regolith thickness instability and the formation of tors in arid environments

Mark W. Strudley,[1] A. Brad Murray,[1] and Peter K. Haff[1]

Received 7 September 2005; revised 25 January 2006; accepted 3 May 2006; published 30 August 2006.

[1] We present model results suggesting that a physical erosion–bedrock weathering feedback is responsible for the development of isolated bedrock knobs (tors/inselbergs) that often punctuate otherwise smooth pediments of homogeneous basement lithology. Tors and larger, more heavily jointed and morphologically complex exposures, inselbergs, may arise as a consequence of fluctuations in rainfall and sediment transport conditions combined with a bedrock weathering mechanism that depends on regolith thickness. Hydrogeochemical considerations and field observations in arid, granitic environments suggest that the relationship between weathering rate and regolith thickness exhibits a maximum for a finite thickness of cover. We have encapsulated this simple erosion-weathering feedback in a numerical model simulating arid/semiarid landscape evolution that produces low-sloping pediments punctuated by tors. Tors form during periods of higher effective moisture, resulting in local base level incision and regolith thinning on pediments, invoking a transition in which mantled surfaces lower at rates exceeding the bare bedrock weathering rate. This condition favors the emergence and growth of tors in areas covered by regolith thickness less than a threshold value. Subsequent shifts in climate or local base level that restore sediment surface lowering rates less than the bare bedrock weathering rate will lead to a progressive decrease in tor height and, ultimately, their disappearance. Thus, according to this model, tors in arid environments represent possibly transient features related to fluctuations in climate or local transport conditions rather than palimpsests of an ancient landscape derived from differential subsurface weathering followed by regolith stripping.

Citation: Strudley, M. W., A. B. Murray, and P. K. Haff (2006), Regolith thickness instability and the formation of tors in arid environments, *J. Geophys. Res.*, *111*, F03010, doi:10.1029/2005JF000405.

1. Introduction

[2] The study of the origins of granitic tors and inselbergs has captivated geologists for over a century. While it is clear that many positive relief elements arise from tectonic activity or by differential weathering and erosion as a result of lithologic or mineralogic variability [*Twidale and Bourne*, 1998; *Twidale and Romani*, 1994], rock masses protruding from beneath a sediment mantle in lithologically homogeneous landscapes remain enigmatic. Many workers propose a two-stage, etching hypothesis in which differential, structurally controlled, subsurface weathering followed by regolith stripping exposes competent granitic masses of low joint density [*Beauvais et al.*, 2003; *Falconer*, 1911; *King and Fair*, 1944; *Linton*, 1955; *Oberlander*, 1972; *Ruxton and Berry*, 1961; *Thomas*, 1965, 1989; *Twidale*, 1962, 1981; *Twidale and Bourne*, 1998; *Twidale and Romani*, 1994; *Willis*, 1936], which may then grow by a positive feedback in which bare rock sheds water to its surrounding, eroding regolith [*Twidale and Bourne*, 1998]. Morphologically more complicated forms such as the flared and stepped granitic bornhardts in the Wheat Belt of southwest Western Australia are said to require multiple, two-stage etching cycles [*Twidale and Bourne*, 1998].

[3] Field observations from pediment passes in the Mojave Desert, California [*Oberlander*, 1972], and from aqueduct tunnels in the Valley of a Thousand Hills in Natal, South Africa [*King*, 1977], however, reveal no difference in joint density between higher standing tors or inselbergs and intervening bedrock floors, suggesting that structure-related differential weathering is not responsible for tor formation in these environments. To expose tors and pediments in the Mojave Desert, the two-stage hypothesis invokes piedmont regolith stripping of Tertiary weathering profiles promoted by vegetation loss and increased erosion rates spurred by the onset of aridity [*Oberlander*, 1974]. Evidence that pediment formation has persisted into the Quaternary [*Dohrenwend*, 1994], combined with observations of a uniformly thin (**O**(m)) regolith layer and gentle slopes ($\sim 5^\circ - 10^\circ$) that both vary little in magnitude across different pediments [*Dohrenwend*, 1994; *Howard*, 1942; *Sharp*, 1957] suggest a dynamic origin for both pediments and tors, rather than an

[1]Division of Earth and Ocean Sciences, Nicholas School of the Environment and Earth Sciences, Center for Nonlinear and Complex Systems, Duke University, Durham, North Carolina, USA.

0148-0227/06/2005JF000405

unearthing. Cosmogenic radionuclide measurements of ^{10}Be taken along vertical profiles of granitic tors in the humid/temperate Bega River Basin in southeastern Australia suggest a model of steady state tor emergence in which the ground surface erosion rate exceeds the tor erosion rate by over threefold [*Heimsath et al.*, 2000], challenging the ubiquity of the two-stage hypothesis.

[4] Most workers, including those favoring the two-stage etching hypothesis [*Thomas*, 1965; *Twidale and Bourne*, 1998], appreciate the accelerating effect that sediment cover has on bedrock weathering rates, as initially suggested by *Gilbert* [1877] and elaborated by *Carson and Kirkby* [1972] in a qualitative, functional form. Additionally, case hardening of exposed rock by a varnish of iron and/or manganese oxides is often cited as reinforcing the efficiency with which bare rock surfaces shed water and escape more rapid disintegration once they become exposed [*Oberlander*, 1972]. However, only a limited number of workers have suggested a feedback between sediment transport behavior and bedrock weathering in initiating tor emergence and promoting tor growth [*Anderson*, 2002; *Carson and Kirkby*, 1972; *Strudley et al.*, 2006; *Wahrhaftig*, 1965]. Importantly, our work builds upon these earlier theoretical foundations by examining numerically how sediment transport and bedrock weathering interact in a landscape evolution model to produce tors, and by testing which climatic and tectonic (base level history) conditions favor tor development on pediments. *Anderson* [2002] has examined the case of tor formation along ridge crests in the high alpine environments of the Laramide ranges of the western United States by producing 1-D numerical simulations of regolith thickness instability induced by slope-driven frost creep at areas of high curvature. We compliment this work by investigating the case of tor development on granitic pediments in arid/semiarid environments where we hypothesize that concentrated fluvial erosion on local or regional scales drives regolith thickness instability. This requires a 2-D (both horizontal dimensions) numerical treatment to examine how an evolving drainage network modifies regolith thickness on pediments, and how spatially complex patterns of fluvial incision, runoff infiltration, and slope-driven "diffusive" smoothing compete to produce either regolith-mantled surfaces or tors.

[5] We have previously shown how smooth bedrock 'pediment' surfaces in granitic desert environments covered by a thin and nearly uniform blanket of regolith emerge spontaneously in a numerical model coupling bedrock weathering and sediment transport by episodic streams [*Strudley et al.*, 2006]. Figure 1 illustrates how pediment surfaces develop through the regulation of bedrock weathering by regolith thickness, which, in turn, reflects surface erosion rates. For example, when regolith thickness exceeds h_{eq}, bedrock weathering rates are less than sediment surface erosion rates, and thus regolith profiles thin over time. This thinning causes bedrock weathering to accelerate, resulting in an equilibrium regolith thickness ($h \rightarrow h_{eq}$, from right). If regolith thickness falls below h_{eq}, regolith profiles thicken over time, causing bedrock weathering rates to decrease; again, regolith thickness ultimately becomes stable ($h \rightarrow h_{eq}$, from left). In the numerical model developed by *Strudley et al.* [2006], this interaction combined with an erosional, but smooth, alluvial surface leads to pediment formation.

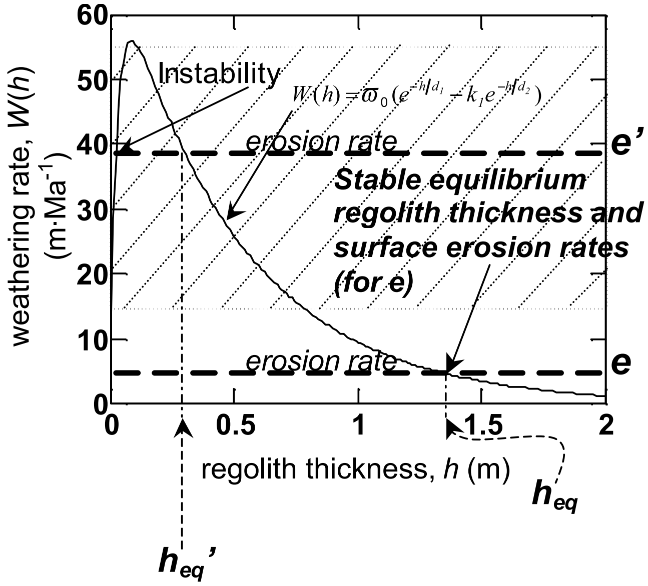

Figure 1. Weathering rate, $W(h)$ (m Ma^{-1}), as a function of regolith thickness, h (m). Parameter values for weathering function are described in text. Dashed lines represent the rate at which alluvial surface is lowering (erosion rates, labeled e and e' (m Ma^{-1})). These erosion rates are determined by sediment flux divergence and boundary conditions; e' represents a domain-averaged pediment denudation rate for the simulation shown in Figure 3. The hatched region represents the range of alluvial surface erosion rates that permit the regolith thickness instability to create tors and extends from the peak of the weathering curve down to the bare bedrock weathering rate of 14 m Ma^{-1}.

[6] Here we provide a test and sensitivity analysis through numerical simulation of the hypothesis that this bedrock weathering–regolith thickness relationship also provides a mechanism for producing spatially variable bedrock exposures (tors and inselbergs) in areas of homogeneous lithology, as originally proposed by *Gilbert* [1877] and *Carson and Kirkby* [1972]. Our model, described below, encapsulates this instability as follows. If surface lowering rates are higher than the bare bedrock weathering rate (hatched area of Figure 1), thinning of the regolith can trigger an instability leading to exposure of bare bedrock. Climate fluctuations, which may manifest themselves as periods of higher effective moisture (decadal to millennial timescales) and changes in local base levels, may cause mantled surfaces to lower at rates exceeding the bare bedrock weathering rate (erosion rates increasing from e to e', which alters the equilibrium regolith thickness on pediments from h_{eq} to h_{eq}', Figure 1). With a mantled surface lowering at such a rate, the form of the weathering rate curve predicts that when regolith thickness falls below a threshold value (see "Instability" in Figure 1), the regolith will approach a stable attractor at zero thickness. If this instability is triggered in a spatially heterogeneous pattern related to ephemeral stream patterns, for example, a tor field will tend to develop. Incipient tors will then grow due to accelerated denudation on mantled surfaces compared to bare rock surfaces. As the tors grow in height, they will also

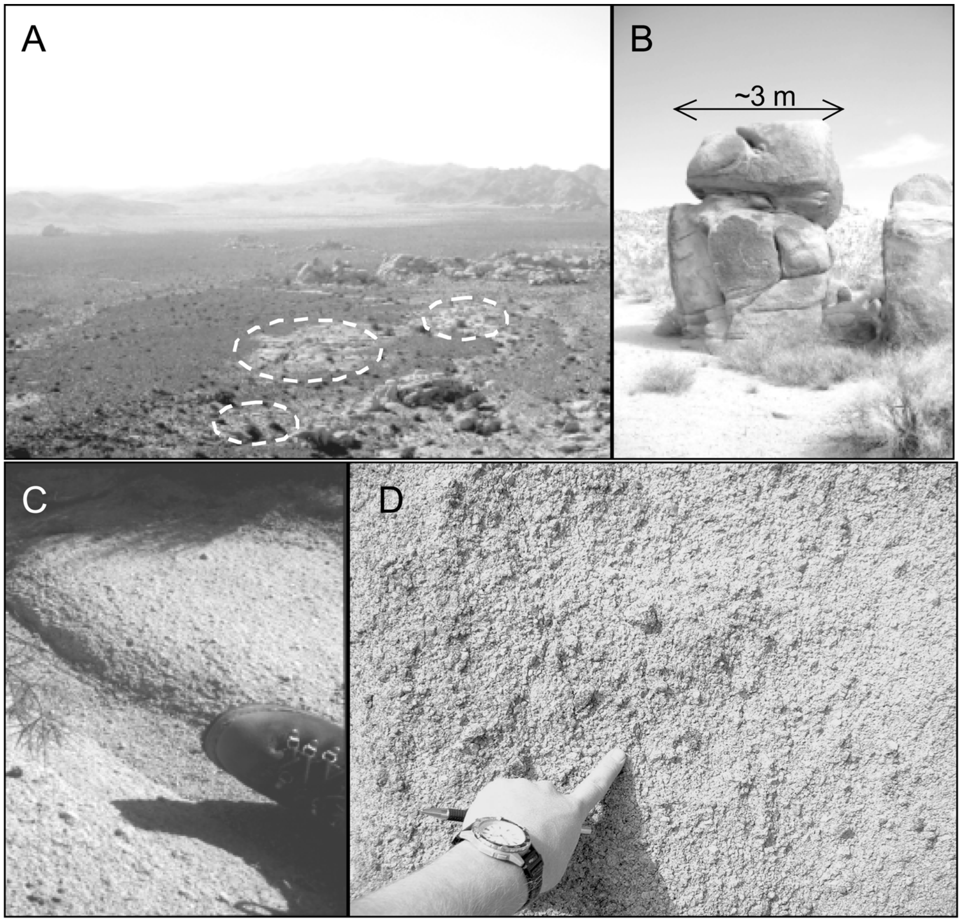

Figure 2. (a) Tors and inselbergs in Joshua Tree National Park, California, just NW of the Ryan Mountains. Dashed ovals in foreground circumscribe "bedrock flats" (~20–30 m in diameter) and low-relief tors, which are kept bare and may have originated by focused stream erosion along channels exiting the Ryan Mountains and flowing roughly northwestward (toward background) into Lost Horse Valley, whose side slopes are pedimented. Note the angular junctions between the higher standing tors and surrounding pediment. (b) Isolated tor in the Mojave Desert, California. Sediment-mantled plain surrounding tor is a pediment surface. (c) Exposed bedrock along stream channel floor in Mojave Desert, California, exhibiting grain-by-grain disintegration and no fluvial sculpting or abrasion. (d) Predominant style of weathering on tor surfaces, illustrating incipient release of plagioclase and quartz grains from granitic groundmass via weathering.

tend to develop the steep sides and angular junctions with the surrounding pediment that characterize classic tor fields found in the Mojave Desert, California, such as those on the flanks of Cima Dome or in Joshua Tree National Park (Figures 2a and 2b).

[7] Subsequent shifts in climate or local base level that restore sediment surface lowering rates less than the bare bedrock weathering rate (e.g., *e* in Figure 1) will lead to a progressive decrease in tor height, ultimately leading to their disappearance. Tors in these environments thus represent possibly transient features related to fluctuations in climate or local transport conditions.

[8] In the work of *Strudley et al.* [2006], numerical simulations produce pediment landforms in hydrologically open and closed basins (the former simulating a bounding stream; the latter simulating an aggrading depositional basin) that lack tors and inselbergs. The absence of tors in these simulations reflects a geometrical constraint imposed by base level conditions that are either fixed or aggrading: low-sloping pediments in these simulations may minutely adjust their longitudinal profiles, pivoting about a fixed (open basin) or rising (closed basin) base level to reflect local sediment transport conditions. The pediment, however, may not lower faster than the bare bedrock weathering rate because the development of a pediment at the foot of a bare bedrock mountain mass, as simulated by *Strudley et al.* [2006], requires the pediment to denude more slowly than the bare bedrock mountain mass weathers, otherwise a trough would develop above a fixed or rising base level. This geometrical constraint precludes conditions that would favor the regolith thickness instability in the presence of a fixed or aggrading base level. Here, we test the hypothesis that the regolith thickness instability and tor formation require surface denudation rates above the bare bedrock weathering rate, which can result from base level fall and/or temporally varying effective moisture.

[9] To clearly articulate the features we seek to model through numerical simulation, the following section describes numerous "type localities" in the southwestern United States containing well-developed tors and inselbergs that we have used to constrain and test our model design. We then describe the numerical implementation of (1) the bedrock weathering mechanism we hypothesize to be responsible for both pediment and tor formation, (2) rainfall-runoff production, and (3) slope-driven and fluvial sediment transport in our landscape evolution model. We also outline initial and boundary conditions in the model, and include a description of model sensitivity tests we perform to examine how perturbations to rainfall rate, base level incision, initial regolith thickness cover, and sediment transport parameters affect tor development. Our results illustrate the time evolution of tor-studded landscapes and highlight conditions in which tor development begins to break down under various climatic and tectonic (base level history) regimes. Our discussion demonstrates both the capabilities and limitations of our model, and emphasizes how initial bedrock geometry within expansive pediments is unlikely to strongly determine the placement and growth of tors. Our primary objective with this work, however, is to test our hypothesis that the two-stage etching model is not required to produce tors and inselbergs on pedimented landscapes, suggesting that the presence of tors may not represent the remains of an ancient landscape, but may instead indicate a dynamic response to transient climatic or tectonic signals.

2. Study Area

[10] Monzogranite, granodiorite, and adamellite of Mesozoic age dominate the granitoid lithology of the Mojave Desert of southern California [*Miller et al.*, 1991], forming mountain cores, pediment basements, and emergent bedrock outcrops (tors) below mountain fronts or along ridge crests (Figures 2a and 2b). Tors in these environments range from faintly convex exposures level with the surrounding pediment to towers and hillocks ~5 m in height. With increasing size, tors become more heavily jointed and covered by boulders and pockets of sediment occasionally supporting plant life ('inselbergs'). Late Cenozoic tectonic activity in the Mojave Desert is restricted to strike-slip faults accommodating distributed simple shear along en eschelon faults [*Dokka and Travis*, 1990] that do not generally define piedmont junctions or the boundaries between tors/inselbergs and surrounding pediments. Tors may be isolated or form part of an extended tor field characterized by a mixture of intact monoliths and boulders derived from their subaerial disintegration. Grain-by-grain spallation of feldspars and quartz (Figures 2c and 2d) driven by the partial hydration of biotite and plagioclase [*Oberlander*, 1972; *Wahrhaftig*, 1965] produces a well-sorted, coarse grus, 0.5 to 1 mm in diameter [*Nichols et al.*, 2002] with a high infiltration capacity. Disintegration along sheet joints produces tabular slabs, whereas mutually orthogonal joint sets yield boulders that eventually become rounded and can be mistaken for tors once toppled onto mantled pediments. Many exposures are relatively friable, but others are coated with a weathering patina of Fe and Mn oxides that resist breakdown; disintegration of these tors and boulders is accomplished by removal of thin exfoliation sheets, which later disintegrate into grus.

[11] The San Bernardino and Little San Bernardino Mountains shelter the Mojave Desert from most Pacific winter cyclones, and annual rainfall rarely exceeds 100 mm y^{-1} [*Oberlander*, 1972; NOAA, hourly precipitation data, 1999]. Stream flow on piedmont surfaces typically occurs in a network of ephemeral channels with depths of centimeters to decimeters and widths on the order of decimeters to a meter [*Nichols et al.*, 2002; *Sharp*, 1957]. Carbonate development in the soil is minimal, and most surface clasts lack desert varnish. Ephemeral washes are responsible for most downslope sediment transport on piedmont surfaces [*Bull*, 1977], and small mammal burrows disrupt regolith profiles to depths less than or equal to ephemeral channel scour [*Nichols et al.*, 2002]. Downslope transport of sediment particles by rain splash plays a small but significant role in identical and similar arid/semiarid environments where vegetative stabilization and protection are lacking [*Dunne and Aubry*, 1986; *Jyotsna and Haff*, 1997]. All drainages in the Mojave Desert terminate in closed, playa basins.

3. Numerical Model

[12] Our model consists of an 80 × 80 grid of cells 3 m across with cell-centered sediment (regolith) and bedrock elevation and regolith thickness attributes that evolve according to regolith formation, diffusive hillslope sediment transport, and fluvial sediment transport in an environment characterized by ephemeral stream flow [*Strudley et al.*, 2006]. Initial conditions consist of a sinusoidal ridge of amplitude 5 m, width and length of 240 m, mantled with regolith on the order of 1 m thick, and seeded with white noise elevation perturbations on both bedrock and sediment surfaces on the order of 1 m [*Anderson*, 2002; *Howard*, 1994]. The lower boundary condition is "open", meaning that the sediment elevation is either fixed or decreasing, the latter representing incision ($\mathbf{O}(10^{-3}$ m $y^{-1})$). Lateral boundary conditions are periodic and permit fluxes of runoff and sediment, thus eliminating the propagation of boundary condition effects into the model domain, which could potentially alter the evolving landscape form.

[13] Bedrock surfaces are modified through time by weathering processes controlled by the overlying thickness of regolith. We model the production of regolith using a bedrock weathering rule motivated by field observations that suggest that a limited regolith cover enhances the weathering rate relative to bare bedrock [*Anderson*, 2002; *Carson and Kirkby*, 1972; *Cox*, 1980; *Dietrich et al.*, 2003; *Furbish and Fagherazzi*, 2001; *Gilbert*, 1877]:

$$W(h) = \varpi_o \left(e^{-h/d_1} - k_1 e^{-h/d_2} \right), \tag{1}$$

where $W(h)$ is the bedrock weathering rate (m Ma^{-1}), ϖ_o = 70 m Ma^{-1}, h is the sediment thickness (m), d_1 = 0.5 m and d_2 = 0.03 m are decay scaling factors, and k_1 = 0.8 is a dimensionless coefficient that determines the magnitude of the bare bedrock weathering rate relative to ϖ_o (Figure 1). Weathering rate parameters are chosen so that the magnitude and functional form of the weathering curve approximate values obtained by measuring the concentrations of cosmogenic radionuclides as a function of depth below the surface from bedrock samples in similar arid/semiarid environments [*Granger et al.*, 1996, 2001; *Nichols et al.*, 2005] and in other environments possessing granitic and sedimentary tors [*Heimsath et al.*, 1999, 2000; *Wilkinson et al.*, 2005]. This functional relationship between bedrock weathering and regolith thickness highlights the importance of mineral hydration and chemical weathering afforded by water retention in thin layers of regolith cover [*Oberlander*, 1972; *Wahrhaftig*, 1965]. Our observations of grain-by-grain spallation even on bedrock surfaces that experience episodic but large amounts of stream flow (Figure 2c) attest to the prevalence and importance of weathering compared to fluvial abrasion and incision. In addition, pockets of sediment which fill small divots on top of and along the periphery of low-amplitude tors consistently cover more friable bedrock than adjacent bare exposures, confirming cosmogenic radionuclide data and the hypothesis that a thin regolith cover enhances weathering rates.

[14] We calculate runoff across our model domain based on rainfall intensity and duration, and infiltration. We seek to simulate realistic arid/semiarid rainfall and storm properties by selecting effective storm intensities, i (m h^{-1}) and durations, t (h storm^{-1}) using hourly precipitation records for stations in the Mojave Desert, California (Baker, Iron Mountain, Mojave, Needles, Victorville) and Bakersfield, California (NOAA, hourly precipitation data, 1999). Likewise, the number of storms per year, n, is constrained by these precipitation records or by randomly selecting n from a normally distributed probability density function (PDF) with mean and standard deviation constrained by the precipitation records. The mean and standard deviation vary between and during simulations, within the ranges: μ = 4–13 storms y^{-1}; σ = 1–10 storms y^{-1}. The PDF-derived rainfall forcing provides an additional sensitivity test of tor development through simulations that experience variable amounts of rainfall through time, some of which may not be sufficient to instigate regolith thickness instability and tor growth.

[15] Infiltration plays a role in damping a downslope increase in runoff magnitude with drainage area, thus its calculation is pertinent in determining runoff fluxes along desert piedmonts. We calculate infiltration depths explicitly at the timescale of individual storms by using a rearrangement of the Green-Ampt equation [*Bedient and Huber*, 1992], which predicts the depth of infiltration reached prior to surface saturation:

$$F = -\psi_f(\theta_s - \theta_u)/(1 - i/K_s), \tag{2}$$

where F is the infiltration depth that occurs implicitly over the course of a storm (m), ψ_f is the wetting front soil suction head (m), θ_s is the saturated sediment porosity, θ_u is the unsaturated sediment porosity, and K_s is the saturated hydraulic conductivity (m h^{-1}) of the sediment. Infiltrated water is assumed to ultimately evaporate, consistent with the absence of perennial streams in the desert environments considered here. Parameter values are from tabulated data based on sand-sized particles [*Bedient and Huber*, 1992]: ψ_f = −0.05 m, θ_s = 0.4, θ_u = 0, and K_s = 0.03 m h^{-1}. When $i \le K_s$, rainfall infiltrates until the regolith column's porosity is exceeded or until the rainfall is completely absorbed. When $i > K_s$, we compare the calculated infiltration depth, F, and the available pore space in the regolith column ($h \cdot \theta_s$), which is limited by local regolith thickness. If the pore space presents no limit to the calculated infiltration depth, F infiltrates. Otherwise, a volume infiltrates per unit area that is equal to the available pore space, with the remaining water, if any, contributing to runoff. Runoff out of each cell for both scenarios ($i \le K_s$ and $i > K_s$) is then

$$q_w = it\Delta x - \min(F\Delta x, h\theta_s\Delta x) + q_n, \tag{3}$$

where q_w is the volumetric runoff per unit width per storm (m^2 storm^{-1}), q_n is the volumetric runoff per unit width per storm arriving in the cell from upstream neighbors (m^2 storm^{-1}), and Δx is the cell size (m). This calculation of runoff allows us to model Hortonian and saturation overland flow in regolith mantled domains, while on bare bedrock there is no infiltration. The model discharges represent summations over the total discharges in channels that are implicit within each cell.

[16] Cells are sorted by elevation and are subjected, in order of descending elevation, to sediment transport processes. Across each nearest-neighbor cell boundary, diffusive transport moves sediment downslope [*Fernandes and Dietrich*, 1997] according to:

$$q_{s,d} = k_2 S, \tag{4}$$

where $q_{s,d}$ is the volumetric sediment flux per unit width (m^2 y^{-1}), S is slope between the centers of adjacent cells, and k_2 is the diffusivity (1 × 10^{-3} m^2 y^{-1}) [*Hanks et al.*, 1984].

[17] Fluvial sediment transport distributes sediment fluxes proportional to slope and runoff [*Carson and Kirkby*, 1972; *Howard*, 1994; *Vanoni*, 1975]:

$$q_{s,f} = k_3 {q_w}^{\alpha} S^{\beta}, \tag{5}$$

where $q_{s,f}$ is the volumetric sediment flux per unit width per storm (m^2 storm^{-1}), k_3 is a transport efficiency parameter, and α and β are constants (k_3 = 1 × 10^{-3} m$^{2-2\alpha}$ storm$^{-(\alpha-1)}$, 1.2 ≤ α ≤ 2.0, β = 1 in runs reported here). The form of this sediment transport rule has been widely used by geomorphologists in landscape evolution models [e.g., *Haff*, 2001; *Howard*, 1994; *Willgoose et al.*, 1991] and has been shown to closely approximate a mean temporal sediment transport relation derived from the instantaneous Einstein-Brown sediment transport formulae originally used for bed load transport in flumes [*Willgoose et al.*, 1991]. Our transport efficiency parameter and exponential constants fall within the range of values used in previous landscape evolution models [e.g., *Haff*, 2001; *Howard*, 1994; *Tucker and Slingerland*, 1997; *Willgoose et al.*, 1991], where 1.0 ≤ α ≤ 2.0 and 1.0 ≤ β ≤ 3.0), although our transport efficiency parameter may assume a value that deviates from others by orders of magnitude due to differences in simulated environment (including the treatment and magnitudes of rainfall rates and runoff development) and variations to the formulae (incorporation of drainage area or shear stress in place of q_w). We calibrated

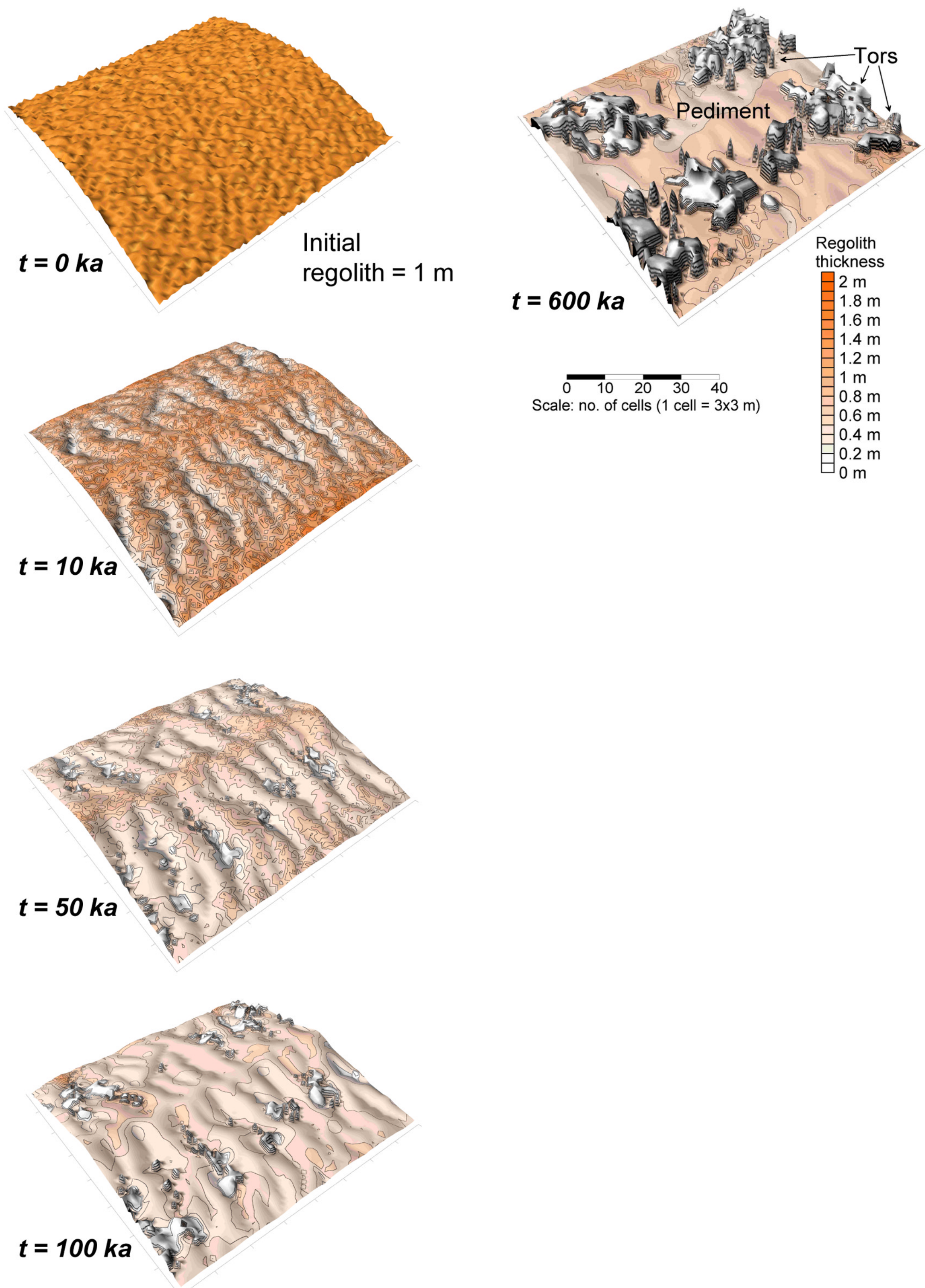

Figure 3. Time slices of simulations illustrating tor development. Color scale for evolving regolith thickness and horizontal scale bar apply to all panels. See text for a description of model initial conditions. Here the lower boundary condition is "open," with the sediment elevation there decreasing, representing base level incision (**O**(10^{-3} m y^{-1})). Simulation uses constant rainfall conditions (64 cm y^{-1}). Tors tend to develop along runoff flow paths initially, but their correspondence to preexisting channel incision (e.g., t = 50 kA) becomes weak as the system evolves (t = 600 kA; compare with Figure 5d).

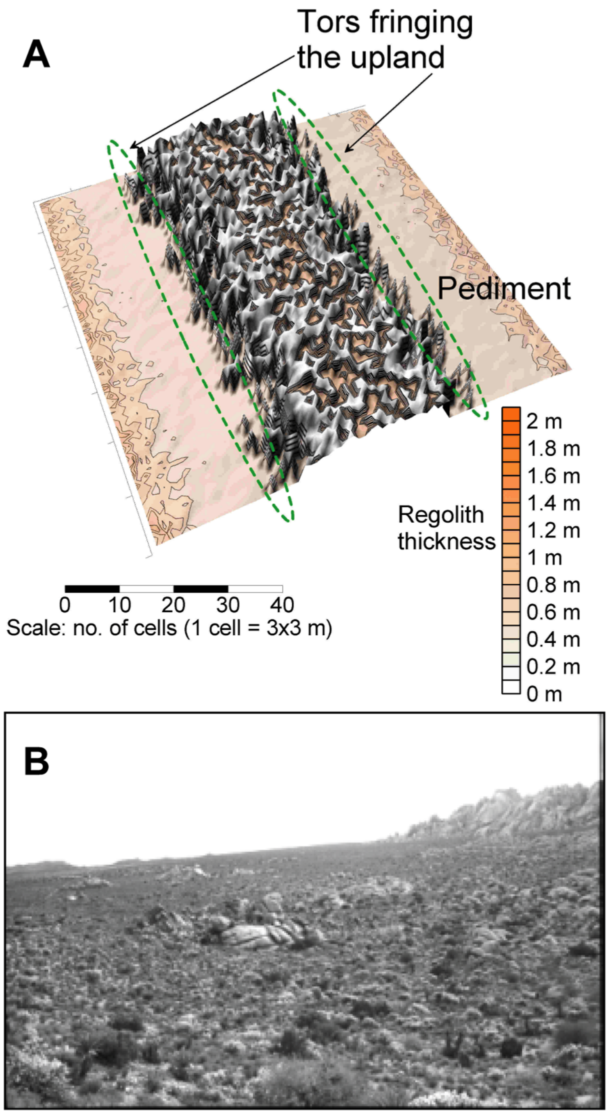

Figure 4. (a) Simulation results illustrating tor growth (dashed green ellipses) fringing a mountain core that is associated with the initial bedrock topographic roughness, not focused stream incision. (b) Illustration showing tors increase in spatial density closer to the Granite Mountains, Mojave Desert, California. Note that the placement of these tors is not well correlated to the local drainage network.

our transport efficiency parameter so that the relief between swales and subtle interfluves is on the order of a meter, as we have observed on Mojave Desert pediments, and the overall pediment lowering rate (with open, nonincisive boundary conditions) is $\sim$10 m Ma^{-1} [*Dohrenwend*, 1994; *Nichols et al.*, 2005]. Hydraulic routing is performed according to the D∞ algorithm of *Tarboton* [1997].

[18] We multiply the sediment fluxes for each storm by the number of storms per year (n) and by the time step (2 years). Here n ranges between 1 and 30, i = 0.04 m h^{-1}, and t = 2.0 h storm^{-1}, modeling the infrequent but geomorphically effective storms occurring on an annual basis in both arid and semiarid grassland environments that have characterized the southwestern United States over the recent geologic past [*Axelrod*, 1950]. We treat sediment erosion and deposition as if they were distributed evenly throughout a cell, reflecting the long timescales of the model and the tendency for channels on pediments to migrate laterally [*Nichols et al.*, 2002]. Sediment surface elevations are adjusted according to the difference of diffusive and advective fluxes in and out of each cell, while bedrock elevations are decreased according to the weathering rule $W(h)$.

[19] We perform numerous simulations using a variety of initial regolith thicknesses, sediment transport conditions, and rainfall and base level incision rates to test the sensitivity of our model of tor development to different climatic and tectonic perturbations. Specifically, we simulate average annual rainfall rates ranging from 30–2400 mm y^{-1}, base level incision rates ranging from 0.00045–9.0 m y^{-1}, initial regolith thickness ranging from 0–5 m, diffusivities (k_2) ranging from 0.0001–0.01 m^2 y^{-1}, transport efficiencies (k_3) ranging from 0.0001–0.01 m$^{2-2\alpha}$ $\cdot$ storm$^{-(\alpha-1)}$, and $1.2 \leq \alpha \leq 2.0$. Because our explanation of tor development requires a climatic change manifested as increased piedmont-wide erosion rates, we have included in our analysis an additional test simulation of tor field development that models rainfall magnitudes (storms y^{-1}) and base level incision rates using a 567,700-year time series of δ^{18}O taken from vein calcite in Devil's Hole cavern in south central Nevada [*Winograd et al.*, 1992]. We employ these data as a "local" wetness proxy because of its remarkable correlation with benthic and planktonic records of paleotemperature [*Crowley*, 1994], which are likely to be positively correlated with effective moisture during the Plio-Pleistocene and Holocene in the southwestern United States [*Axelrod*, 1944; *Axelrod*, 1950; *van Devender*, 1977; *van Devender and Spaulding*, 1979; *Wells et al.*, 1987]. We use the δ^{18}O record as a basis of correlation for a linear interpolation and extrapolation of rainfall and base level incision rates during the period of record (567,700 y), assuming rainfall rates during the Last Glacial Maximum (LGM, $\sim$21,000 yBP) were double the current magnitude (100 mm y^{-1} [*van Devender and Spaulding*, 1979]) and base level incision rates varied from 0.4 mm y^{-1} during the LGM to 0 mm y^{-1} at present [*Nichols et al.*, 2002]. The magnitude of base level incision during the LGM was chosen arbitrarily, although tor development in the model is insensitive to the magnitude chosen and only requires that portions of the record produce base level incision rates that support pediment denudation rates above the bare bedrock weathering rate.

4. Results

[20] Our simulations illustrate the development of bedrock exposures that develop over a period of 600 kA, creating up to $\sim$5 m of relief above mantled pediments (e.g., Figures 3–5). Figure 3 illustrates the time evolution of tor development on a pedimented landscape over the course of 600 kA. Tors in this simulation initially begin their growth relative to surrounding mantled surfaces between 10 and 50 kA at locations where concentrated stream flow has thinned the regolith profile beyond the threshold regolith thickness, initiating the instability in which the bedrock becomes uncovered. This timescale represents the time needed for bedrock weathering rates and sediment surface

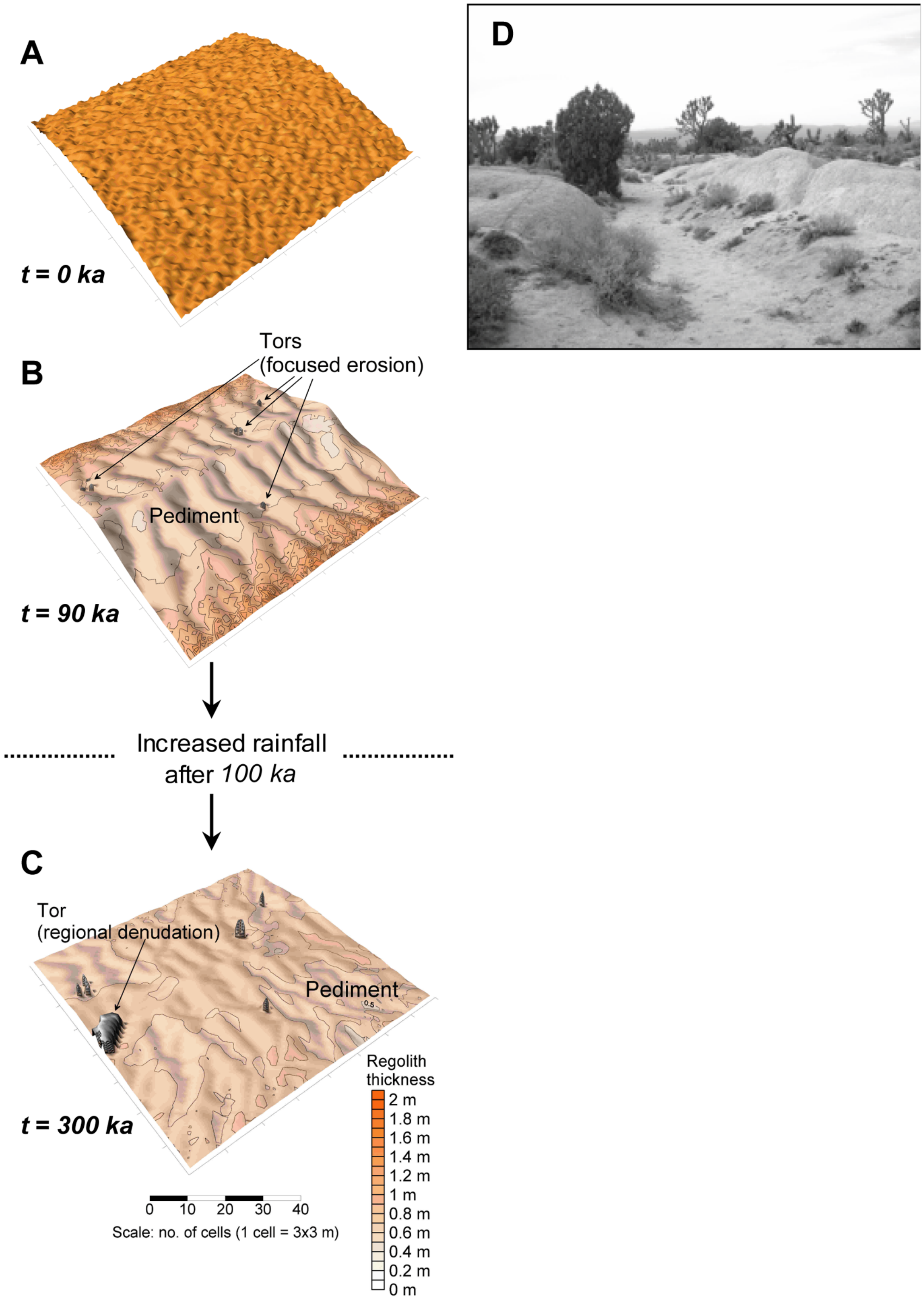

Figure 5. Time slices of simulations illustrating tor development from both focused stream incision and regional denudation associated with increased rainfall. Color scale for evolving regolith thickness and horizontal scale bar apply to all panels. (a) Initial condition. See text for a description of model initial conditions. (b) Tor growth through the regolith thickness instability initiated by focused runoff and incision (after 90 ka). (c) Plot showing that following a step function increase in rainfall at 100 ka, a large tor grows at the landscape crest due to adjustment of the pediment slope in response to higher amounts of runoff. (d) Tors on interfluves near the apex of Cima Dome, Mojave Desert, California.

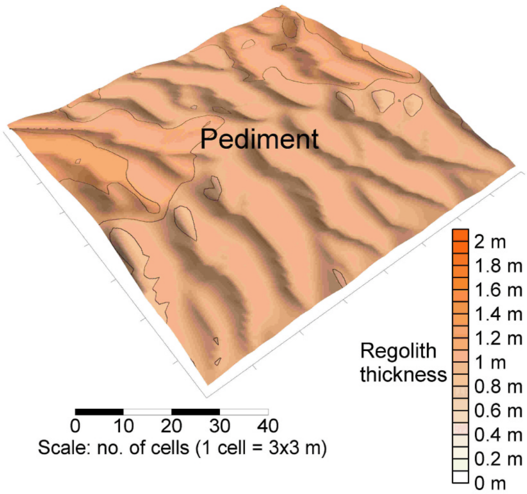

Figure 6. Simulation illustrating lack of tor development despite base level incision of 0.0003 m y^{-1}. Pediment denudation rates do not exceed the bare bedrock weathering rate. Model duration is 500 kA.

erosion rates to equilibrate, and will be determined by the initial regolith thickness and the magnitudes of bedrock weathering and physical erosion processes. The precise location of tor development is dependent on initial white noise elevation perturbations and areas of high curvature to the extent that these deviations from a smooth surface determine runoff flow paths and areas of regolith thinning that initiate the regolith thickness instability. Figure 3, for example, also illustrates that in some cases tors may not grow along the ridge crest or near mountain cores because the downslope accumulation of runoff is not sufficient to cause incision beyond the threshold regolith thickness at these locations on the landscape. Once exposed on the landscape, tors then evolve according to the bare bedrock weathering rate, whereas adjacent mantled areas lower at rates defined by sediment transport conditions and the equilibrium regolith thickness. In this scenario, tors develop as significant bedrock protuberances after exposure, and not in the subsurface.

[21] Tors may also grow along the ridge crest or near mountain cores when increased rainfall and runoff rates induce a decline in pediment slopes that cause headward thinning of regolith profiles, inducing the regolith thickness instability (Figures 4 and 5). In these cases, the regolith thickness instability is not associated with localized areas of concentrated fluvial incision. Figure 4a illustrates the results from a simulation in which initial rainfall and runoff rates were sufficiently high to create pediment slopes that exposed an initially buried (1 m of regolith) bedrock crest. This rainfall rate also favored pediment denudation rates above the bare bedrock weathering rate, causing initial bedrock irregularities near the exposed bedrock crest to grow relative to mantled areas once they became exposed. Figures 5a–5c show time slices of simulation results illustrating how step function increases in rainfall rates may induce headward thinning of regolith profiles and growth of tors in response to the regolith thickness instability. In this simulation, concentrated fluvial incision (Figure 5b) and regional regolith thinning (Figure 5c) both create tors. Figures 4b and 5d show examples from the Granite Mountains and Cima Dome, Mojave Desert, California, respectively, that potentially represent analogues to these simulations; tors are exposed preferentially toward ridge crests and do not generally correspond to drainage patterns. We wish to emphasize through both the simulations and field observations shown in Figures 4 and 5 that the mechanisms that initiate the regolith thickness instability and tor growth are varied, and can be related to either localized or regional regolith thinning by fluvial activity.

[22] Tors tend to persist in our modeled landscape because they form areas of local relief that efficiently shed rain and divert stream flow, perpetuating the difference in lowering rates between rapidly denuding, mantled pediments and slowly weathering, bare bedrock tors. Although piedmont incision is subdued by the diffusive nature of fluvial sediment transport in these environments [*Strudley et al.*, 2006], an irregular patchwork of tors develops from the chaotic, disconnected channel systems that characterize granitic piedmonts [*Sharp*, 1957].

[23] An aggradational base level tends to inhibit tor development. With a closed boundary condition, the lower portions of the landscape are strictly depositional. The upper portions eventually become erosional, but with small lowering rates. Barring extreme increases in precipitation/runoff that would rapidly reduce the slopes, the small lowering rates prevent the regolith thickness instability. With fixed elevation lower boundary conditions and constant rainfall/runoff rates, mantled areas become graded to base level and are geometrically and dynamically restricted to lower at rates less than the bare bedrock weathering rate, regardless of rainfall and runoff rates (Figure 6) [*Strudley et al.*, 2006]. Tor development in the model requires either: (1) a base level incision rate that produces pediment denudation rates above the bare bedrock weathering rate or (2) an increase in precipitation/runoff that lowers mantled slopes and/or increases the lowering rate of upper portions of the surface beyond the bare bedrock weathering rate.

[24] The appearance of tor fields in the model is robust against large variations in annual rainfall (30–2400 mm y^{-1}), the degree of nonlinearity in fluvial sediment transport as a function of discharge (α = 1.2–2.0), the thickness of the initial regolith cover (0.0–5.0 m), the base level incision rate ($\geq$0.45 mm y^{-1}), and the fluvial sediment transport efficiency (0.0001–0.01 $m^{2-2\alpha}$ $storm^{-(\alpha-1)}$). The system is moderately insensitive to fluctuations in diffusivity (0.0001–0.01 m^2 y^{-1}), with lower values favoring tor development. Figures 7 and 8 illustrate a series of simulations summarizing our sensitivity analysis of tor development in light of these climatic and tectonic perturbations, while Table 1 defines baseline model parameter values, initial conditions, and boundary conditions from which perturbations deviate in our sensitivity analysis. Figures 7a and 7b illustrate tor field development under conditions of hyperaridity (Figure 7a; 30 mm y^{-1} annual rainfall) and under rainfall rates corresponding to temperate/humid conditions (Figure 7b; 2400 mm y^{-1}). Increasing the rainfall rate increases the spatial frequency with which fluvial sediment transport is able to achieve regolith thinning beyond the threshold value necessary to induce the instability leading to tor growth. The "hyperarid" simulation

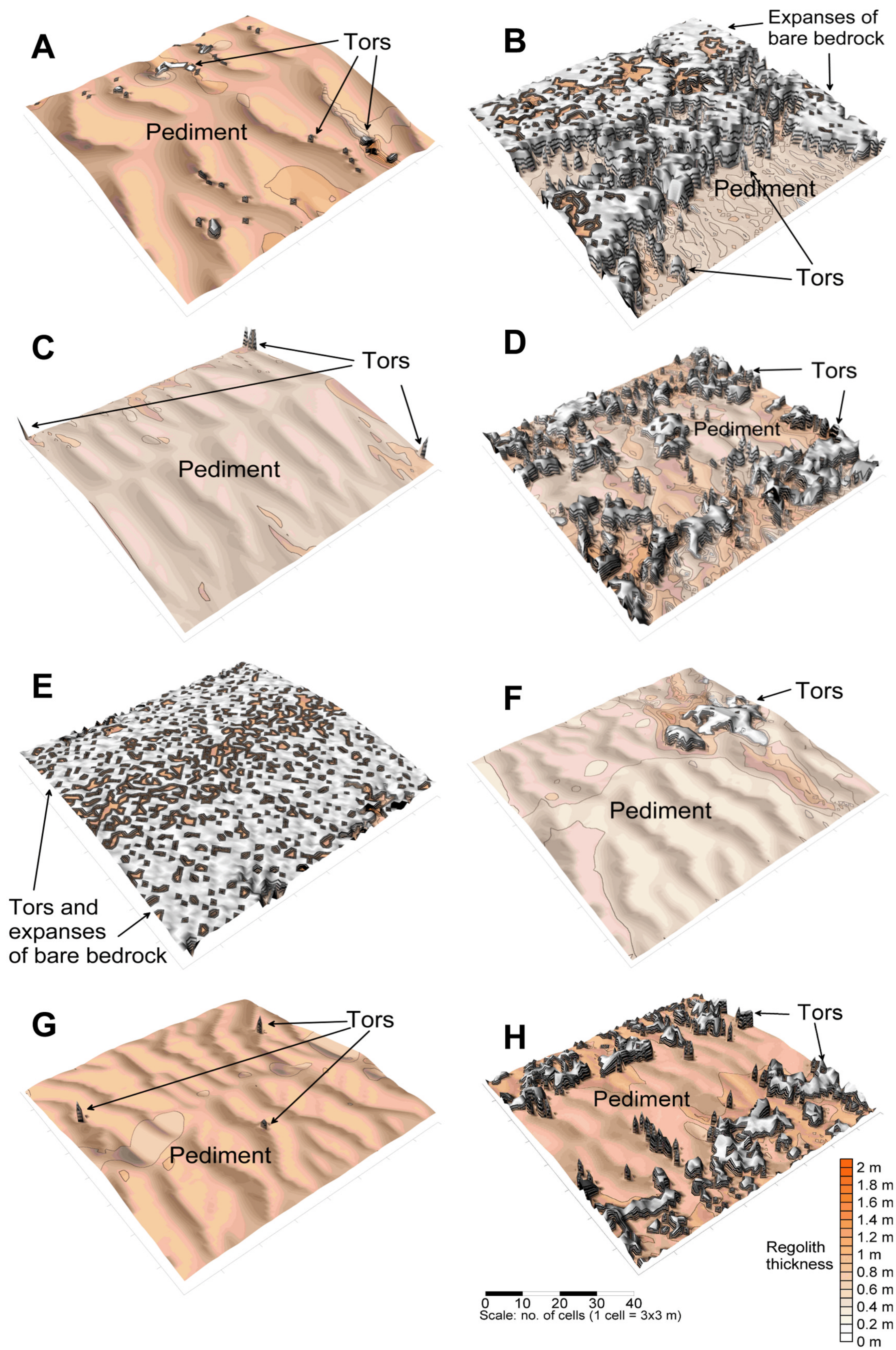
A
Tors
Pediment
B
Expanses of bare bedrock
Pediment
Tors
C
Tors
Pediment
D
Tors
Pediment
E
Tors and expanses of bare bedrock
F
Tors
Pediment
G
Tors
Pediment
H
Tors
Pediment
0 10 20 30 40
Scale: no. of cells (1 cell = 3x3 m)
Regolith thickness
2 m
1.8 m
1.6 m
1.4 m
1.2 m
1 m
0.8 m
0.6 m
0.4 m
0.2 m
0 m

Figure 7

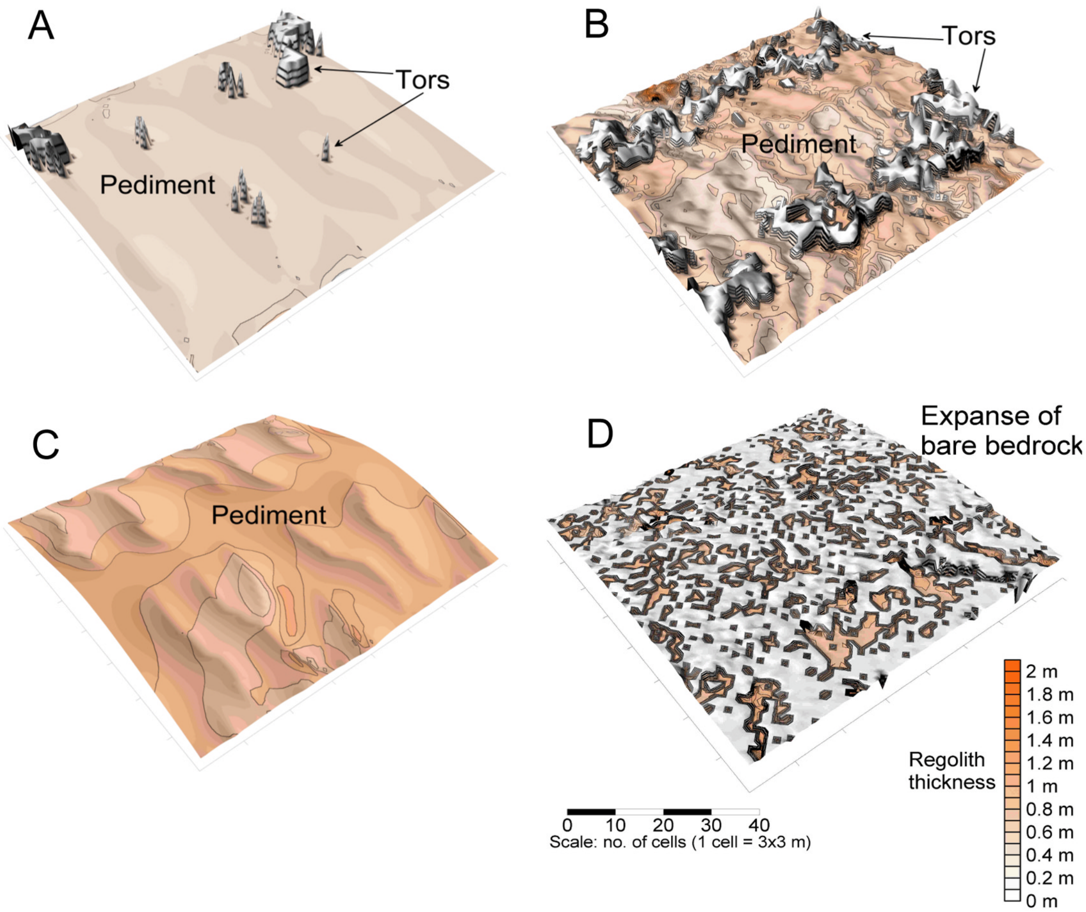

Figure 8. Results of sensitivity analysis of tor development (600 kA model duration). See text and Table 1 for a description of model initial and boundary conditions and parameter values. Differences in topography are derived from various initial conditions and/or rainfall and base level incision rates that create various denudation histories. Color scale for evolving regolith thickness and horizontal scale bar shown in Figure 8d apply to all panels. Simulation results using a diffusivity (k_2; equation (4)) of (a) 1×10^{-2} m^2 y^{-1} and (b) 1×10^{-4} m^2 y^{-1}. Simulation results using a transport efficiency (k_3; equation (5)) of (c) 1×10^{-4} m$^{2-2\alpha}$ storm$^{-(\alpha-1)}$ and (c) 1×10^{-2} m$^{2-2\alpha}$ storm$^{-(\alpha-1)}$.

exhibits tors along the flanks of the ridge, while the large amounts of runoff generated in the ‘‘humid’’ case permit tor development along the flanks of the landscape as well as at the ridge crest, including wholesale stripping of the regolith along certain portions of the landscape.

[25] Increasing the degree of nonlinearity in fluvial sediment transport as a function of discharge (α, equation (5)) from 1.2 (Figure 7c) to 2.0 (Figure 7d) increases the interfluve spacing, which yields a landscape with higher drainage density and more rapid relaxation of the initial sinusoidal ridge because of higher runoff and erosion rates. The tor field in the more ‘‘nonlinear’’ case is better developed and covers a greater portion of the landscape than for the ‘‘weakly nonlinear’’ case. Weakly nonlinear fluvial sediment transport (Figure 7c) is only able to produce tors near the downslope boundary of the model domain where runoff accumulation is sufficient to induce the instability. In contrast, a highly nonlinear fluvial sediment transport rule creates both isolated bedrock knobs as well as larger expanses of bedrock exposures that may be more aptly termed inselbergs (Figure 7d).

[26] Figures 7e and 7f illustrate simulation results with initial regolith thicknesses of 0 and 5 meters, respectively. With an initial regolith thickness below values corresponding

Figure 7. Results of sensitivity analysis of tor development (600 kA model duration). See text and Table 1 for a description of model initial and boundary conditions and parameter values. Differences in topography derive from various initial conditions and/or rainfall and base level incision rates that create various denudation histories. Color scale for evolving regolith thickness and horizontal scale bar shown in Figure 7h apply to all panels. Simulation results using constant rainfall conditions of (a) 30 mm y^{-1} and (b) 2400 mm y^{-1}. Simulation results using (c) $\alpha = 1.2$ (equation (5)) and (c) $\alpha = 2.0$. Simulation results for an initial regolith thickness of (e) 0 m and (f) 5 m. Simulation results using a base level incision rate of (g) 0.45 mm y^{-1} and (h) 9 m y^{-1}.

Table 1. Model Parameter Values, Initial Conditions, and Boundary Conditions for Basic Case of Tor Development[a]

	Value
Initial geometry	Sine ridge
Amplitude	5 m
Wavelength	480 m
Model domain	240 × 240 m
Lateral boundary conditions	periodic
Base level incision rate	0.0012 m y^{-1}
$h_{initial}$	1 m
Δx	3 m
ϖ_o	70 m Ma^{-1}
d_1	0.5 m
d_2	0.03 m
k_1	0.8
i	0.04 m h^{-1}
t	2.0 h $storm^{-1}$
n	4 storms y^{-1}
ψ_f	−0.05 m
θ_s	0.4
θ_u	0
K_s	0.03 m h^{-1}
k_2	$1{\cdot}10^{-3}$ m^2 y^{-1}
k_3	1×10^{-3} $m^{2-2\alpha}$ $storm^{-(\alpha-1)}$
α	1.2
β	1

[a]See Figure 3.

to peak weathering rates (∼10 cm; Figure 1), local fluctuations in lowering rate drive most areas to the stable attractor at 0 m regolith thickness (Figure 1), leading to a mostly bare bedrock surface. Pockets of regolith form and persist in local areas of deposition related to the initial white noise elevation perturbations of the bedrock surface. These pockets of sediment are slightly more prevalent near the ridge crest because insufficient runoff and low slopes at the crest limit sediment transport rates. For initially thick regolith cover (5 m; Figure 7f), tor field development proceeds more slowly, with far fewer tors developing across the landscape than in the basic case (Figure 3) at a given time step. Continuing landscape evolution in this simulation (not shown) yields more tors as a greater portion of the surface reaches an equilibrium regolith thickness that is susceptible to the instability.

[27] Figures 7g and 7h show how tors develop under widely varying base level incision rates: 0.45 mm y^{-1} in Figure 7g and 9 m y^{-1} in Figure 7h. Tors predictably become more numerous for landscapes experiencing higher rates of base level incision, which encourages regolith thinning, regolith thickness instability, and tor growth. Provided that climatic conditions foster pediment denudation rates exceeding the bare bedrock weathering rate, base level incision rates may be increased ad infinitum without completely stripping the pediment of its regolith. This occurs because slowly eroding, bare bedrock benches that form at the model boundaries decouple mantled pediments above from boundary incision, preserving an arid landscape analogue to the high alpine surfaces modeled by *Anderson* [2002]. In contrast to Anderson's model, however, tors here may form anywhere in the landscape rather than primarily at the crest. Our regolith thickness instability is initiated in areas of concentrated regolith thinning or stream flow, which tend to occur at a finite distance from the divide, whereas instabilities in Anderson's model are related to

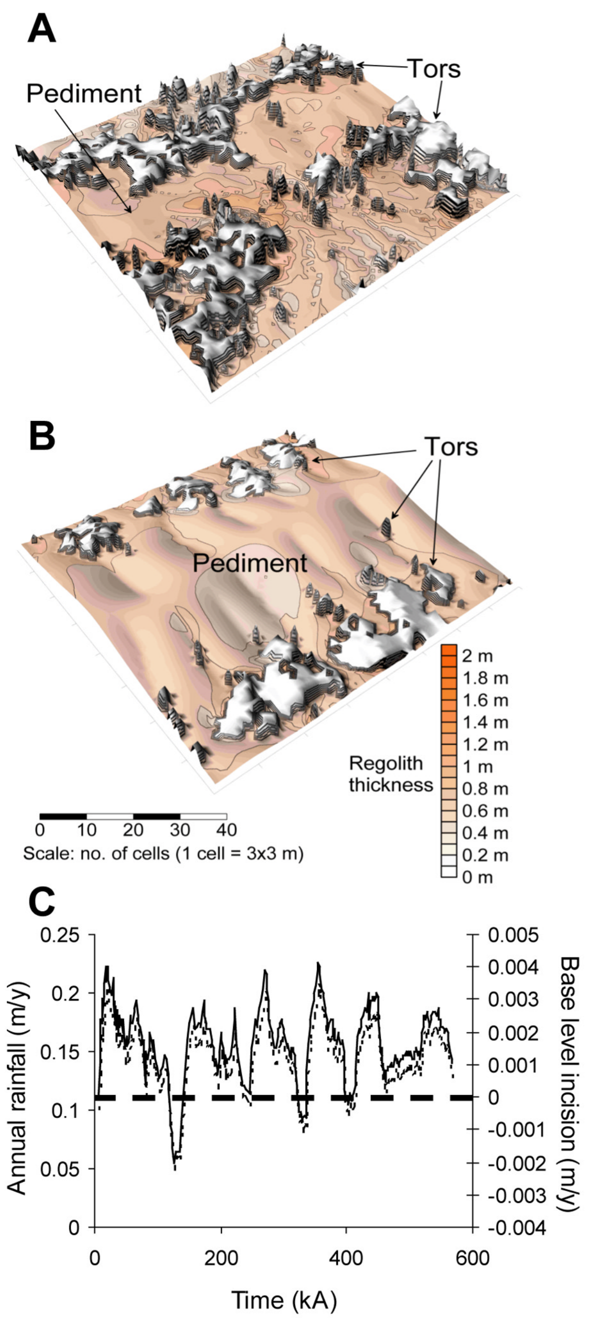

Figure 9. (a) Simulation results using rainfall amounts selected from a normally distributed PDF (μ = 5 storms y^{-1}, σ = 2 storms y^{-1}; duration is 500 kA). (b) Simulation results using rainfall and base level incision rates constrained by $\delta^{18}O$ record from vein calcite, Devil's Hole cavern, Nevada (includes both fixed elevation and incisive boundary conditions (O(10^{-4} m y^{-1}))). Initial sinusoidal ridge amplitude is 10 m. Regolith thickness and horizontal scale bars apply to both Figures 9a and 9b. (c) Time series of rainfall (dashed line) and base level incision rates (solid line) (m y^{-1}) derived from the Devil's Hole $\delta^{18}O$ record used to drive model shown in Figure 9b. Region below the thick dashed line highlights effective negative base level incision rates, which are modeled as a closed, aggradational base level.

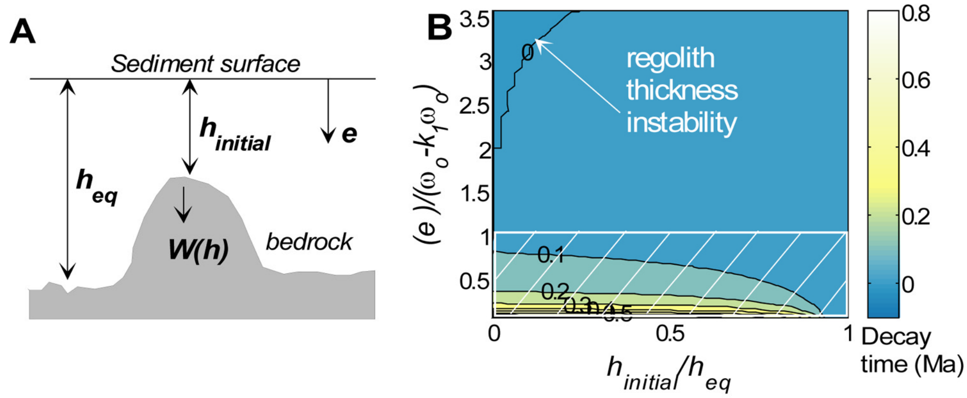

Figure 10. (a) Conceptual diagram of a 1-D model of bedrock and alluvial surface evolution used to derive (b) subsurface decay times for bedrock irregularities of various geometries. Decay times represent the time necessary for a bedrock knob in the subsurface to decay to an elevation equivalent to the adjacent bedrock (i.e., the time necessary for the regolith thickness to reach 95% of its equilibrium value, h_{eq}). Parameter h_{eq} is an equilibrium regolith thickness from Figure 1; $h_{initial}$ represents various initial differences between alluvial surface and top of bedrock knob. Contour surface (Figure 10b) plots decay times as a function of relief normalized by h_{eq} (which varies according to denudation rate) and surface denudation rates normalized by the bare bedrock weathering rate, $\omega_o - k_1\omega_o = 14$ m Ma^{-1}. Hatched region shows conditions under which the proposed regolith thickness instability is inoperative. In the far top left, decay times approach zero and become negative, representing tor growth through the instability.

areas of high topographic curvature and accelerated frost creep at ridge crests and at bedrock lips that bound the model domain.

[28] Adjusting the diffusivity (k_2, equation (4)) through two orders of magnitude (0.0001–0.01 m^2 y^{-1}) does alter the style of tor development (Figures 8a and 8b), with higher values of k_2 (0.01 m^2 y^{-1}) suppressing tor growth by reducing the efficiency of fluvial incision and regolith thinning. Although modeling endeavors of various slope-driven sediment transport processes have utilized an equivalent range of diffusivities [*Fernandes and Dietrich*, 1997; *Martin*, 2000], rates on the order of 0.001 m^2 y^{-1} have been used in previous studies examining scarp diffusion for sediment types that approximate the field conditions we seek to model [*Hanks et al.*, 1984], and cosmogenic radionuclide data of soil production rates across a range of climatic and tectonic environments imply sediment diffusivities of this magnitude [*Heimsath et al.*, 2005].

[29] Adjustments to the fluvial sediment transport efficiency term (k_3, equation (5)) through two orders of magnitude (0.0001–0.01 m$^{2-2\alpha}$ storm$^{-(\alpha-1)}$), shown in Figures 8c and 8d, illustrate how a reduction in k_3 to 0.0001 m$^{2-2\alpha}$ storm$^{-(\alpha-1)}$ prevents tor growth while increasing k_3 to 0.01 m$^{2-2\alpha}$ storm$^{-(\alpha-1)}$ yields nearly complete removal of the regolith profile from the entire landscape. For the latter, fluvial erosion outpaces bedrock weathering processes except at localized areas associated with sediment deposition in small hollows created by the initial random perturbation field to the bedrock topography.

[30] Finally, the appearance of tor fields is also robust against temporal fluctuations in storm size (Figure 9a) and coupled variations in storm size and base level incision (Figure 9b) constrained by wetness proxy data based on a 567,700-year time series of δ^{18}O taken from vein calcite in Devil's Hole cavern in south central Nevada [*Winograd et al.*, 1992]. Figure 9c shows the time series for both rainfall and base level incision rates derived from this record, and highlights the times during which base level aggradation occurs in the model (below thick dashed line in Figure 9c). In both cases, tors persist in the landscape despite experiencing either (1) rainfall and runoff rates insufficient to invoke conditions in which the regolith thickness instability may be achieved (erosion rates drop below the bare bedrock weathering rate; *e* in Figure 1) or (2) zero base level incision (aggradation).

[31] Although our model permits the exposure of preexisting subsurface bedrock irregularities, which may later grow into tors, our analysis suggests that subsurface bedrock topographic heterogeneity decays relatively rapidly (Figure 10), favoring a laterally uniform equilibrium regolith thickness that is characteristic of pediments [*Strudley et al.*, 2006]. We arrive at this conclusion by constructing a 1-D model of bedrock and alluvial surface evolution, which we use to derive subsurface decay times (Figure 10b) for bedrock irregularities of various geometries (Figure 10a). In this model, decay times represent the time necessary for a bedrock knob in the subsurface to decay to an elevation equivalent to the adjacent bedrock surface (i.e., the time necessary for the regolith thickness to reach 95% of its equilibrium value, h_{eq}). The model subjects subsurface bedrock irregularities of various heights ($h_{eq} - h_{initial}$; h_{eq} is an equilibrium regolith thickness from Figure 1; $h_{initial}$ represents various initial differences between the alluvial surface and the top of a bedrock knob) to various surface denudation rates (***e***) for a fixed bedrock weathering function, *W*(h) (see Figure 1 and equation (1)). The contour surface in Figure 10b plots these decay times as a function of the relief of these bedrock knobs normalized by h_{eq} (which varies according to denudation rate) and surface denudation rates normalized by the bare bedrock weathering

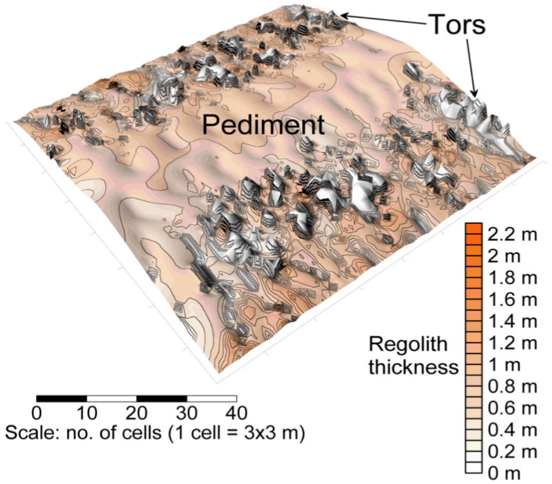

Figure 11. Simulation of tor development where storm footprints vary through time in size and placement across the landscape. Infiltration of runoff and sediment deposition outside of storm footprints does not prevent tor formation for rainfall rates defined in Table 1. Model duration is 500 kA.

rate, $\omega_o - k_1\omega_o = 14$ m Ma^{-1}. The hatched region shows conditions under which the proposed regolith thickness instability is inoperative, because the normalized denudation rate is less than unity (exposed bare bedrock would weather faster than sediment surfaces erode, precluding tor development). Note that this area also corresponds to the only domain in Figure 10b for which subsurface decay times are large, representing the only situation in this 1-D model for which subsurface knobs would persist, to potentially be exposed as tors. Most decay times (outside of the hatched area) are on the order of 10^0–10^2 years. For subsurface "knobs", the regolith thickness instability may theoretically be initiated in the nonhatched domain, but becomes increasingly important toward the upper left portion of the plot, where subsurface bedrock irregularities are close to the surface and denudation rates are high. In the far upper left, decay times approach zero and become negative, representing tor growth through the regolith thickness instability.

5. Discussion

[32] Because the size of the smallest tors produced in the model is on the order of the model's cell size, 3 × 3 m, we cannot address the minimum area of bedrock exposure necessary for tor growth. Simulations incorporating spatially limited storm footprints with random sizes and locations (Figure 11) do not hinder the development of tors anywhere in the landscape despite the potential of local deposition downhill of storm footprints because of waning overland flow. The paucity of tors in granitic desert environments of the southwestern United States smaller than a few meters across may suggest a lower limit and motivates our choice of cell size in the model. At the opposite end of the spectrum, some large inselbergs may be remnants of separated mountain spurs derived from the disintegration of divides that once linked these promontories to larger mountain masses, yet our simulations produce landscapes ornamented with large inselberg forms up to ~30 meters across (Figures 3, 7b, 7d, 7h, and 8b). This result seems consistent with the apparently recent exposure of large bedrock "flats" from local stream flow at the base of the Ryan Mountains in Joshua Tree National Park, CA (Figure 2a, foreground).

[33] Our model of tor development requires minor shifts in climate that accelerate local erosion and base level incision rates. The existence of incised, tor-studded pediments abutting the Granite Mountains (~34°50′00″N; ~115°40′00″W) in the Mojave Desert, along with cosmogenic radionuclide-derived measurements of sediment transport rates suggesting a cessation of piedmont deposition in the late Pleistocene [*Nichols et al.*, 2002], may reflect the manifestation of such a climatic shift.

[34] Tor development in our model, however, does not require weathering rates or sediment production to respond to climate. Recent work indicating that long-term hillslope sediment production only weakly responds to nonglacial climate changes in granitic environments [*Riebe et al.*, 2001a] suggests that Pleistocene and Holocene moisture fluctuations should not strongly affect the regolith thickness instability responsible for tor development in our model. More importantly, chemical weathering rates and the rate at which fresh rock is supplied to regolith profiles appears to be weakly correlated to climate and strongly controlled by tectonics [*Riebe et al.*, 2001b, 2004]. Because the uplift of the San Bernardino Mountain Ranges established the present atmospheric circulation patterns in the Mojave Desert at the close of the Pliocene [*Oberlander*, 1972], the extent to which climatic and tectonic perturbations have modified weathering and erosion rates over the timescales of tor growth in our model are inconsequential in the context of tor development.

[35] The work of *Wilkinson et al.* [2005] provides cosmogenic radionuclide data that support the form of a "humped" weathering curve, as used in our model, for heath and forest-covered ferruginized sandstone hillslopes in the Blue Mountains of southeastern Australia that are accented by bare bedrock outcrops and "pagodas". They propose, however, that the high-standing sandstone "pagoda tors" are resistant corestones that exhibit rapid weathering rates characteristic of a state of decay rather than growth. In contrast, low-relief bedrock outcrops at this site reflect slower weathering rates than mantled areas, but *Wilkinson et al.* [2005] suggest that these features are unlikely to persist and grow into high-amplitude tors because a spatially shifting vegetation mosaic in the long term, as evidenced by the maintenance of low-relief, heath-covered surfaces during landscape lowering, produces a monotonically decaying exponential relationship between bedrock weathering and regolith thickness. Field relationships at Mojave Desert sites exhibit both low- and high-amplitude tors that do not appear to correspond to consistent trends in mineralogy or structure, nor does it appear that vegetation plays a significant role in regolith production on desert pediments.

[36] Our model of tor development involves testable predictions about the relationships between rates of bedrock weathering and pediment surface lowering (and base level lowering). Specifically, our model predicts that (1) tor exposure history should reflect constant regolith thickness, constant regolith production, and constant tor weathering

rates, (2) the present-day height of intact tors should reflect a constant exposure history, and (3) tor development should correspond to a local base level incision history commensurate with local regolith production and sediment transport rates. Measurements of cosmogenic radionuclide (both ^{10}Be and ^{26}Al) concentrations on and adjacent to tors coupled with piedmont base level incision rate estimates will provide data for future model tests of tor development for site-specific cases. Although base level incision rates are difficult to measure in the field, inverse modeling exercises using (1) cosmogenic radionuclide concentrations of in-stream or channel-bank bedrock samples, (2) optically stimulated luminescence of piedmont deposits, or (3) piedmont pedogenic relationships may provide appropriate data to constrain base level history.

6. Conclusion

[37] Classic models of tor development invoke tectonic activity, differential weathering and erosion as a result of lithologic or mineralogic variability, or a two-stage, etching hypothesis in which differential, structurally controlled, subsurface weathering followed by regolith stripping exposes competent granitic masses of low joint density. Field observations and cosmogenic radionuclide data, however, have not consistently supported these models of tor development, nor has any attempt yet been made to describe tor field development in a numerical modeling context in arid/semiarid environments.

[38] Here we have described a numerical model that provides a plausible mechanism to explain arid region tor development in areas of homogeneous lithology. These landform elements arise autogenically, because of a basic regolith thickness bedrock weathering instability, combined with fluctuations in rainfall and sediment transport conditions. Tor development in the model requires either (1) a base level incision rate that produces pediment denudation rates above the bare bedrock weathering rate or (2) an increase in precipitation/runoff that lowers mantled slopes and/or increases the lowering rate of upper portions of the surface beyond the bare bedrock weathering rate. Our model suggests that tors may be an inherently nonsteady state phenomenon, altering between growth and decay as climate shifts. Tors self-organize in our model in the sense that they arise from the interactions within the system; there is no external template that dictates their existence or spatial arrangement. Thus perturbations in climate and sediment transport may ultimately drive the evolution of bare bedrock protrusions where spatially varying lithology or structure is unimportant.

[39] **Acknowledgments.** This manuscript greatly benefited from the comments of two anonymous reviewers, which ultimately led to a substantial reorganization of the text. We also wish to thank Thomas Crowley for discussions regarding climatic variability in the southwestern United States and for directing us to pertinent climatic data sets for use in our model. We thank members of the Surface Processes Club at Duke University for discussions that stimulated this work. The U.S. Army Research Office [DAAD19-99-1-0191] and the Andrew W. Mellon Foundation provided partial support.

References

Anderson, R. S. (2002), Modeling the tor-dotted crests, bedrock edges, and parabolic profiles of high alpine surfaces of the Wind River Range, Wyoming, *Geomorphology*, *46*, 35–58.

Axelrod, D. (1944), The Pliocene sequence in central California, in *Pliocene Floras of California and Oregon*, edited by R. W. Chaney, pp. 207–224, Carnegie Inst. of Wash., Washington, D. C.

Axelrod, D. (1950), Evolution of desert vegetation, in *Studies in Late Tertiary Paleobotany*, pp. 215–306, Carnegie Inst. of Wash., Washington, D. C.

Beauvais, A., M. Ritz, J.-C. Parisot, and C. Bantsimba (2003), Testing etching hypothesis for the shaping of granite dome structures beneath lateritic weathering landsurfaces using ERT method, *Earth Surf. Processes Landforms*, *28*, 1071–1080.

Bedient, P. B., and W. C. Huber (1992), *Hydrology and Floodplain Analysis*, 692 pp., Addison-Wesley, Reading, Mass.

Bull, W. B. (1977), The alluvial-fan environment, *Prog. Phys. Geogr.*, *1*, 222–270.

Carson, M. A., and M. J. Kirkby (1972), *Hillslope Form and Process*, Cambridge Univ. Press, New York.

Cox, N. J. (1980), On the relationship between bedrock lowering and regolith thickness, *Earth Surf. Processes Landforms*, *5*, 271–274.

Crowley, T. J. (1994), Potential reconciliation of Devils Hole and deep-sea Pleistocene chronologies, *Paleoceanography*, *9*(1), 1–5.

Dietrich, W. E., D. G. Bellugi, L. S. Sklar, J. D. Stock, A. M. Heimsath, and J. J. Roering (2003), Geomorphic transport laws for predicting landscape form and dynamics, in *Prediction in Geomorphology*, *Geophys. Monogr. Ser.*, vol. 135, edited by P. R. Wilcock and R. M. Iverson, pp. 103–132, AGU, Washington, D. C.

Dohrenwend, J. C. (1994), Pediments in arid environments, in *Geomorphology of Desert Environments*, edited by A. D. Abrahams and A. J. Parsons, pp. 321–353, CRC Press, Boca Raton, Fla.

Dokka, R. K., and C. J. Travis (1990), Late Cenozoic strike-slip faulting in the Mojave Desert, California, *Tectonics*, *9*, 311–340.

Dunne, T., and B. F. Aubry (1986), Evaluation of Horton's theory of sheetwash and rill erosion on the basis of field experiments, in *Hillslope Processes*, edited by A. D. Abrahams, pp. 31–53, Allen and Unwin, St. Leonards, N. S. W., Australia.

Falconer, J. D. (1911), *The Geology and Geography of Northern Nigeria*, 286 pp., MacMillan, New York.

Fernandes, N. F., and W. E. Dietrich (1997), Hillslope evolution by diffusive processes: The timescale of equilibrium adjustments, *Water Resour. Res.*, *33*, 1307–1318.

Furbish, D. J., and S. Fagherazzi (2001), Stability of creeping soil and implications for hillslope evolution, *Water Resour. Res.*, *37*, 2607–2618.

Gilbert, G. K. (1877), Report on the geology of the Henry Mountains, U.S. Geol. Surv., Reston, Va.

Granger, D. E., J. W. Kirchner, and R. Finkel (1996), Spatially averaged long-term erosion rates measured from in situ produced cosmogenic nuclides in alluvial sediment, *J. Geology*, *104*, 249–257.

Granger, D. E., C. S. Riebe, J. W. Kirchner, and R. Finkel (2001), Modulation of erosion on steep granitic slopes by boulder armoring, as revealed by cosmogenic ^{26}Al and ^{10}Be, *Earth Planet. Sci. Lett.*, *186*, 269–281.

Haff, P. K. (2001), Waterbots, in *Landscape Erosion and Evolution Modeling*, edited by R. S. Harmon, pp. 239–275, Springer, New York.

Hanks, T. C., R. C. Bucknam, K. R. Lajoie, and R. E. Wallace (1984), Modification of wave-cut and fault-controlled landforms, *J. Geophys. Res.*, *89*, 5771–5790.

Heimsath, A. M., W. E. Dietrich, K. Nishiizumi, and R. C. Finkel (1999), Cosmogenic nuclides, topography, and the spatial variation of soil depth, *Geomorphology*, *27*, 151–172.

Heimsath, A. M., J. Chappell, W. E. Dietrich, K. Nishiizumi, and R. C. Finkel (2000), Soil production on a retreating escarpment in southeastern Australia, *Geology*, *28*, 787–790.

Heimsath, A. M., D. J. Furbish, and W. E. Dietrich (2005), The illusion of diffusion: Field evidence for depth-dependent sediment transport, *Geology*, *33*(12), 949–952.

Howard, A. D. (1942), Pediment passes and the pediment problem, *J. Geomorphol.*, *5*, 3–32, 95–136.

Howard, A. D. (1994), A detachment-limited model of drainage basin evolution, *Water Resour. Res.*, *30*, 2261–2285.

Jyotsna, R., and P. K. Haff (1997), Microtopography as an indicator of modern hillslope diffusivity in arid terrain, *Geology*, *25*, 695–698.

King, L. C. (1977), What bornhardts teach, *Z. Geomorphol.*, *21*(3), 366–367.

King, L. C., and J. D. Fair (1944), Hillslopes and dongas, *Trans. Proc. Geol. Soc. S. Afr.*, *47*, 1–4.

Linton, D. L. (1955), The problem of tors, *Geogr. J.*, *121*, 470–487.

Martin, Y. (2000), Modelling hillslope evolution: Linear and nonlinear transport relations, *Geomorphology*, *34*(1–2), 1–21.

Miller, D. M., R. J. Miller, J. E. Nielson, H. G. Wilshire, K. A. Howard, and P. Stone (1991), Preliminary geologic map of the East Mojave National Scenic Area, California, *U.S. Geol. Surv. Open File Rep., 91–435*, 8 pp.

Nichols, K. K., P. R. Bierman, R. L. Hooke, E. M. Clapp, and M. Caffee (2002), Quantifying sediment transport on desert piedmonts using ^{10}Be and ^{26}Al, *Geomorphology*, *45*, 105–125.

Nichols, K. K., P. R. Bierman, M. Caffee, R. Finkel, and J. Larsen (2005), Cosmogenically enabled sediment budgeting, *Geology*, *33*, 133–136.

Oberlander, T. M. (1972), Morphogenesis of granitic boulder slopes in the Mojave Desert, California, *J. Geol.*, *80*, 1–20.

Oberlander, T. M. (1974), Landscape inheritance and the pediment problem in the Mojave Desert of southern California, *Am. J. Sci.*, *274*, 849–875.

Riebe, C. S., J. W. Kirchner, D. E. Granger, and R. Finkel (2001a), Minimal climatic control on erosion rates in the Sierra Nevada, California, *Geology*, *29*, 447–450.

Riebe, C. S., J. W. Kirchner, D. E. Granger, and R. C. Finkel (2001b), Strong tectonic and weak climatic control of long-term chemical weathering rates, *Geology*, *29*, 511–514.

Riebe, C. S., J. W. Kirchner, and R. Finkel (2004), Erosional and climatic effects on long-term chemical weathering rates in granitic landscapes spanning diverse climatic regimes, *Earth Planet. Sci. Lett.*, *224*, 547–562.

Ruxton, B. P., and L. Berry (1961), Weathering profiles and geomorphic position on granite in two tropical regions, *Rev. Geomorph. Dyn.*, *12*(1), 16–31.

Sharp, R. P. (1957), Geomorphology of Cima Dome, Mojave Desert, California, *Geol. Soc. Am. Bull.*, *68*, 273–290.

Strudley, M. W., A. B. Murray, and P. K. Haff (2006), The emergence of pediments, tors, and piedmont junctions from a bedrock weathering-regolith thickness feedback, *Geology*, in press.

Tarboton, D. G. (1997), A new method for the determination of flow directions and upslope areas in grid digital elevation models, *Water Resour. Res.*, *33*, 309–319.

Thomas, M. F. (1965), Some aspects of the geomorphology of domes and tors in Nigeria, *Z. Geomorphol.*, *9*, 63–81.

Thomas, M. F. (1989), The role of etch processes in landform development: I. Etching concepts and their applications, *Z. Geomorphol.*, *33*, 129–142.

Tucker, G. E., and R. Slingerland (1997), Drainage basin responses to climate change, *Water Resour. Res.*, *33*, 2031–2047.

Twidale, C. R. (1962), Steepened margins of inselbergs from north-western Eyre Peninsula, South Australia, *Z. Geomorphol.*, *6*, 51–69.

Twidale, C. R. (1981), Inselbergs-exhumed and exposed, *Z. Geomorphol.*, *25*, 219–221.

Twidale, C. R., and J. A. Bourne (1998), Origin and age of bornhardts, southwest Western Australia, *Aust. J. Earth Sci.*, *45*, 903–914.

Twidale, C. R., and J. R. V. Romani (1994), On the multistage development of etch forms, *Geomorphology*, *11*, 107–124.

van Devender, T. R. (1977), Holocene woodlands in the southwestern deserts, *Science*, *198*, 189–192.

van Devender, T. R., and W. G. Spaulding (1979), Development of vegetation and climate in the southwestern United States, *Science*, *204*, 701–710.

Vanoni, V. A. (1975), *Sedimentation Engineering*, *Manu. Rep. Eng. Pract.*, vol. 54, 745 pp., Am. Soc. of Civ. Eng., Reston, Va.

Wahrhaftig, C. (1965), Stepped topography of the southern Sierra Nevada, California, *Geol. Soc. Am. Bull.*, *76*, 1165–1190.

Wells, S. G., L. D. McFadden, and J. C. Dohrenwend (1987), Influence of late Quaternary climatic changes on geomorphic and pedogenic processes on a desert piedmont, eastern Mojave Desert, California, *Quat. Res.*, *27*, 130–146.

Wilkinson, M. T., J. Chappell, G. S. Humphreys, K. Fifield, B. Smith, and P. Hesse (2005), Soil production in heath and forest, Blue Mountains, Australia: Influence of lithology and palaeoclimate, *Earth Surf. Processes Landforms*, *30*, 923–934.

Willgoose, G., R. L. Bras, and I. Rodriguez-Iturbe (1991), A coupled channel network growth and hillslope evolution model: 1. Theory, *Water Resour. Res.*, *27*, 1671–1684.

Willis, B. (1936), *Studies in Comparative Seismology: East African Plateaus and Rift Valleys*, 358 pp., Carnegie Inst. of Wash., Washington, D. C.

Winograd, I. J., T. B. Coplen, J. M. Landwehr, A. C. Riggs, K. R. Ludwig, B. J. Szabo, P. T. Kolesar, and K. M. Revesz (1992), Continuous 500,000-year climate record from vein calcite in Devils Hole, Nevada, *Science*, *258*, 255–260.

P. K. Haff, A. B. Murray, and M. W. Strudley, Division of Earth and Ocean Sciences, Nicholas School of the Environment and Earth Sciences, Center for Nonlinear and Complex Systems, Duke University, Durham, NC 27708, USA. (mws10@duke.edu)